TENTH AUSTRALASIAN FLUID MECHANICS
CONFERENCE - UNIVERSITY OF MELBOURNE
11-15 DECEMBER 1989



# THE PHASE-DEPENDENCE OF A SWIRLING, TURBULENT BOUNDARY LAYER

S.G. KOH, P.D. CLAUSEN and D.H. WOOD

Department of Mechanical Engineering
University of Newcastle, NSW 2308
AUSTRALIA

ABSTRACT

Measurements have been made in a swirling turbulent boundary layer affected by the angular momentum instability. The flow field seen by a rotating observer was obtained from a fixed hot-wire probe using the technique of phase-locked averaging. The instability is localised to the wall region of the boundary layer and there is some evidence that it has produced "streamwise" vortices analogous to the Taylor-Gortler vortices in a boundary layer on a concave wall. The mean velocities and Reynolds stresses show a significant phase dependence which appears to originate in the swirl generator. The conventional Reynolds stresses are not equally affected by the phase dependence and this has implications for the turbulence modelling of swirling flows.

## 1. INTRODUCTION

It is well known that an *inviscid* instability occurs in any curved flow where the angular momentum decreases away from the centre of curvature, eg Townsend (1976). An important and much studied example is the nominally two-dimensional (2-D) boundary layer on a concave wall where the instability results from the no-slip condition. In laminar flow, this leads to the formation of longitudinal Taylor-Gortler vortices with a spanwise wavelength of about twice the boundary layer thickness, $\delta$. Each wavelength contains two counter-rotating vortices. Because the instability is inviscid, it is generally supposed that the same happens in turbulent flow where spanwise variations have been found in the easily-measured surface shear stress, eg Hoffmann *et al.* (1985). The variations depend on upstream conditions, and have a peak-to-peak value of 10 - 20% of the average with a spanwise "wavelength" of about $2\delta$. They have even been found in the boundary layer on the flat walls of a working section downstream of a contraction, which necessarily contains a concave wall, Mehta & Hoffmann (1987).

If the flow is axisymmetric and swirling, the angular momentum vector usually lies in the axial direction, but this should not change the basic instability. However, a new complication is possible: the conventional, time-averaged measurements from a fixed probe may be circumferentially uniform, but similar measurements from a probe rotating with the flow may not. Furthermore, the non-uniformity could be associated with a rotating system of "longitudinal" vortices. This possibility can be examined by sampling a fixed probe on the basis of $\theta_*$, the 'phase' angle between the probe and some arbitrary, but rotating point in the flow. (The symbol $\theta_*$ is used to distinguish the phase angle from the circumferential co-ordinate $\theta$ used often for axisymmetric flows.) Ensemble averages for constant $\theta_*$ are called phase-locked averages (PLA) by Gostelow (1977). They are taken routinely in studies of turbomachinery, eg Laksminarayana (1981), but *not*, as far as we are aware, in swirling flows. PLA measurements for a range of $\theta_*$ should provide information similar to conventional measurements in the nominally two-dimensional flows cited above.

The present experimental apparatus, consisting of a wind tunnel and swirl generator, Fig. 1, is similar to that used by Jacquin *et al.* (1987) to study the effects of rotation on homogeneous turbulence, and by Hagiwara *et al.* (1986) who were primarily interested in the subsequent diffusion of the swirling flow. Measurements made in a diffuser attached to the present swirl generator were reported by Clausen & Wood (1987). The boundary layer on the wall of the swirl generator becomes susceptible to the instability when it encounters the downstream stationary section. There are many similarities to the external flow over an axially-aligned cylinder, when the upstream part of the cylinder is spinning, eg Driver & Hebbar (1987) and references therein. This, and other flows, such as the swirling annular flow of Yowakim & Kind (1988) may well be affected by the angular momentum instability, but, we repeat, the possibility does not appear to have been investigated.

The first major aim of the present experiment is the obvious one of determining the phase-dependent axial vorticity in the unstable boundary layer. Unfortunately, no similar measurements are available for the nominally two-dimensional flows mentioned above, perhaps because of the large amount of extra traversing that would have been required; of course, this is replaced by the much easier PLA for swirling flows. There is also some doubt as to whether clearly defined vorticity contours could be obtained, for the reasons given by Baskaran & Bradshaw (1988) and there are flows where weak longitudinal vorticity is accompanied by large cross-stream changes in the turbulence structure, eg Hooper & Wood (1984). Therefore it is possible that *any* phase-dependence will modify the turbulence structure. In addressing this possibility we restrict attention to the conventional Reynolds stresses, which will be modified if a conventional mean velocity, G say, differs from the PLA mean velocity at any $\theta_*$. Let this difference be $g(\theta_*)$ and let $g(\theta_*, t)$ be the time-dependent fluctuation about $G + g(\theta_*)$. Then the total instantaneous velocity is $G + g(\theta_*) + g(\theta_*, t)$. For the conventional (fixed point) Reynolds decomposition, let g be the time-dependent fluctuation about G, so that the total instantaneous velocity is $G + g$. Now introduce another velocity component with F and f defined analogously to G and g. Since

$$\bar{f} = \bar{g} = \overline{f(\theta_*, t)} = \overline{g(\theta_*, t)} = \langle f(\theta_*) \rangle = \langle g(\theta_*) \rangle = 0$$

it is easy to show that a conventional Reynolds stress, $\overline{fg}$, is related to the average of the phase-dependent stress by

$$\overline{fg} = \langle \overline{f(\theta_*, t)\, g(\theta_*, t)} \rangle + \langle f(\theta_*)\, g(\theta_*) \rangle \qquad (1)$$

The overbar denotes ensemble averaging. The "< >" brackets indicate a phase average over the range $0° \le \theta \le 360°$. The last term in equn (1) contains only *mean*-velocity terms, and so will be called the "phase-dependent mean" term. The second major aim of this work is to determine its effect on the conventional stresses.

Any phase-dependence of the stresses can have significant implications for computational models of swirling flow. For

example, the turbulence energy, k, may be affected differently from the shear stresses. If the two are related, such as by an eddy viscosity in the modelled Reynolds-stress equations, then the relationship may need to depend on the way the phase-dependence is established.

The next section describes the experiment and the measurement techniques and is followed by the Results and Discussion. The two major aims of this work will be addressed together rather than in the sequence implied in this Introduction. The last Section contains the major conclusions.

## 2. EXPERIMENT AND MEASUREMENT TECHNIQUES

The swirl generator is shown in Fig. 1. A 20 mm length of aluminium honeycomb was placed at the start of the rotating section. The cell diameter was 3.2 mm and the wall was 0.025 mm thick, giving an open area ratio of close to 0.97. The downstream flow consisted of nearly-solid-body rotation about the centreline at 130 mm, with a reasonably uniform axial profile outside the boundary layer whose thickness, $\delta$, was 20 mm; $\delta$ was determined as the distance to where U was 0.99% of the average axial velocity $U_0$. These measurements, and the boundary layer results given below were obtained 75 mm downstream of the end of the rotating section. Partly to thicken the boundary layer, and partly to hold the honeycomb in place, Dymo tape was attached to the pipe wall. The tape was inscribed with an endless succesion of (capital) "V"s. The major dimensions of the swirl generator are given in Fig. 1. No screens were placed downstream of the honeycomb. $U_0$ was 12.4 m/s, and the rotational speed of the swirl generator, $\Omega$, was 57.6 rad/s (550 rpm) .

Most measurements were obtained using a DISA 55P51 X-probe with home-made 5 μm tungsten wires, whose active portion of 1.2 mm was isolated from the prongs by copper plated stubs of 20 μm diameter. The probe was operated by constant temperature anemometers similar to those described by Miller *et al.* (1987) and was calibrated for velocity and yaw using the technique developed by Clausen and Wood (1989). The total anemometer voltages were acquired digitally using the system described by Clausen (1988). Subsequently, the King's law calibrations were digitally inverted, so no linearisation was necessary. Measurements were obtained at each radius after rotating the probe into the flow by approximately $\beta = \tan^{-1}(W/U)$, to avoid contamination by the velocities transverse to the plane of the wires. We estimate the general accuracy of the conventional Reynolds stresses at around 10%. This is well within the reproducibility of the normal stresses shown below and is comparable to the accuracy obtained by Anderson & Eaton (1989) who used a very similar X-probe in a three-dimensional (3-D) flow. They give a detailed discussion of the possible measurement errors. The conventional measurements were obtained by sampling at 1 kHz for 30s. To measure the phase-dependent quantities, the data acquisition system was triggered externally once per revolution of the swirl generator. This defined the arbitrary origin for $\theta_*$; subsequent values were inferred from $\Omega$ and the sampling rate. The probe was sampled at 150 values of $\theta_*$ per revolution and the ensemble averages were obtained over 3,000 revolutions of the swirl generator. The first experiment covered about 330° of the possible 360° range of $\theta_*$, to allow estimates to be made of the terms in equn (1). (Obtaining measurements over the full range of $\theta_*$ would have prevented sampling each revolution as well as real-time processing of the data.) In the second experiment, the 150 values of $\theta_*$ covered about 60° to give a resolution in $\theta_*$ comparable to the 1 mm radial steps taken by the hot-wires. This range of $\theta_*$ is equivalent to nearly 8$\delta$ and should, therefore, be sufficiently large to investigate the existence of "streamwise" vortices.

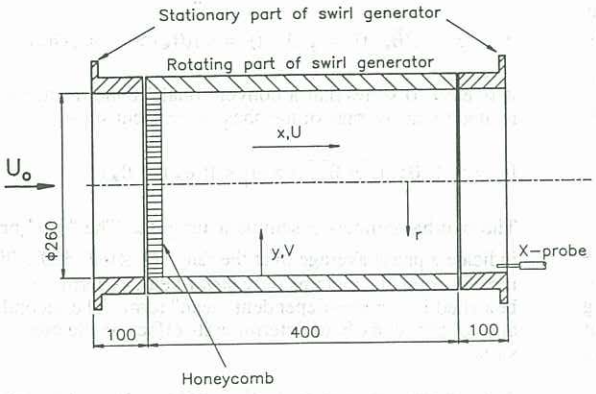


Figure 1. Schematic of swirl generator showing measurement position and co-ordinate system. All dimensions in mm.

A single hot-wire probe was used to measure closer to the wall than was possible with the X-probe. The conventional U and W were obtained by first yawing the probe to find Q, the "total" velocity defined by $Q^2 = U^2 + W^2$. This was done in 5° steps, the large step size being justified by the nearly flat yaw response at small angles. Then the probe was yawed by an additional 40° to find W/U using the more sensitive yaw response at large angles. The phase-dependent U and W were determined in a similar manner, with $Q(\theta_*)$ found from results taken over several 5° steps, stored and then searched for the maximum at each $\theta_*$, in case the angle for $Q(\theta_*)$ varied with $\theta_*$. Note that a single-wire cannot resolve V, which appears in the axial vorticity equation, or *any* of the stresses in the co-ordinates of Fig. 1.

## 3. RESULTS AND DISCUSSION

The conventional U and W close to the wall are shown in Fig. 2 along with Wr to indicate the localisation of the instability to the inner third of the boundary layer. The W results suggest a smaller $\delta$ than do the U measurements because the circumferential boundary layer develops only from the start of the non-rotating section of the swirl generator as an "internal layer" within the previously-formed axial boundary layer. This is typical of the formation of 3-D from 2-D boundary layers, eg Bradshaw (1987) and bears some similarities to the response of a 2-D boundary layer to a change in surface conditions, eg Smits & Wood (1985).

Examples of the conventional turbulence stresses are plotted in Fig. 3. For economy, they are shown together with the independently determined terms in equn (1) which will be considered below. Also shown is the "wall" value of $\overline{vw}$ ,

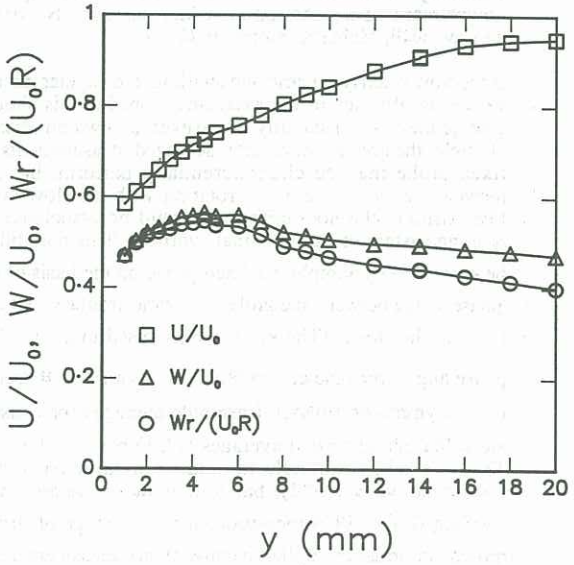


Figure 2. Mean velocities in boundary layer.

obtained by estimating the total wall stress from the Clauser chart for Q, and finding the wall streamline angle by plotting U against W for small y. The angle was 35° to the x-axis and was approximately constant for $y \leq 3$ mm.

As an example of the phase-dependent mean velocities, $W(\theta_*)$ is shown in Fig. 4. The profile at y = 5 mm has a variation of ±4%, and is similar in shape to the single-wire measurements of W closer to the wall. It is, therefore, typical of the profiles in the region where $\partial(Wr)/\partial r$ is negative. Between y = 5 and 10 mm, the shape of the $W(\theta_*)$ changes to such an extent that $W(\theta_*)$ in the outer layer becomes approximately anti-correlated with $W(\theta_*)$ close to the wall. The changes *cannot* be attributed immediately to the instability as such, because they could be just a consequence of the change in sign of $\partial W/\partial y$ as y increases, Fig. 2. If the first order effect of the phase-dependence is to alter δ, without altering its suitability as the relevant local length scale, any phase-dependent perturbation will change sign if the y-gradient of the mean of that quantity changes sign. However, the shape of the $U(\theta_*)$ (which is not shown) for *all* y resembles closely the shape of $W(\theta_*)$ in the *outer* layer, whereas $\partial U/\partial y$ is always positive. (The variations in $U(\theta_*)$ are greater than in $W(\theta_*)$, for example, about ±10% at y = 5 mm.) Thus the phase-dependence cannot be explained entirely as a consequence of variations in δ. Neither can the dependence of the turbulence quantities, of which $\overline{w^2}(\theta_*,t)$ in Fig. 5 is an example. Note that these measurements are phase-averaged to get the first term on the right hand side of equn (1). The shape of $\overline{u^2}(\theta_*,t)$ (not shown) changes appreciably across the boundary layer, tending, with increasing y, from correlation to anti-correlation with $U(\theta_*)$ and the outer-layer $W(\theta_*)$. However, $\overline{w^2}(\theta_*,t)$ does not change in shape and remains approximately correlated with W near the wall (and $\overline{u^2}(\theta_*,t)$ in the outer layer). This difference occurs even though $\partial\overline{w^2}/\partial y$ is always negative as is $\partial\overline{u^2}/\partial y$, except perhaps at y = 7 mm. In summary, a phase-dependence in δ could explain the changes in $U(\theta_*)$, $W(\theta_*)$ and $\overline{w^2}(\theta_*,t)$ as y increases but not those in $\overline{u^2}(\theta_*,t)$. This possibility makes it difficult to isolate the effect of the instability in these measurements.

Fig. 6 shows the phase-dependent axial vorticity contours for the range in $\theta_*$ corresponding to about 6δ; the full range is not shown in the interests of clarity. The 5 mm region where $\partial(Wr)/\partial y < 0$ is equivalent to nearly 2°. The few regions of negative vorticity near the wall are indicated by the arrows. It is immediately obvious that there are no strong axial vortices with scales comparable to δ, probably because of the restriction of the instability to the inner part of the boundary layer, which could not be traversed extensively with an X-probe. In this region there is some evidence for vortices in the form of contours that presumably would be closed by more extensive measurements. There is a similar localisation of axial vorticity in the calculations by Floryan (1989) for curved wall jets where the instability is also localised. Interestingly, the "vortices" in Fig. 6 do not appear to be counter-rotating and so are more like the co-rotating vortices formed from the cross-flow instability, eg Reed & Saric (1989). It must be noted, however, that this instability is caused by a cross-stream (in this case circumferential) pressure gradient and so should not be important here.

Fig. 3 shows the application of equn (1) to $\overline{u^2}$ and $\overline{vw}$. The three terms in the equation were obtained independently from the conventional measurements, which should equal the sum of the two terms on the right hand side of equn (1). There is excellent agreement in all three normal stresses, indicating that phase-averaging over only 330° did not introduce any serious

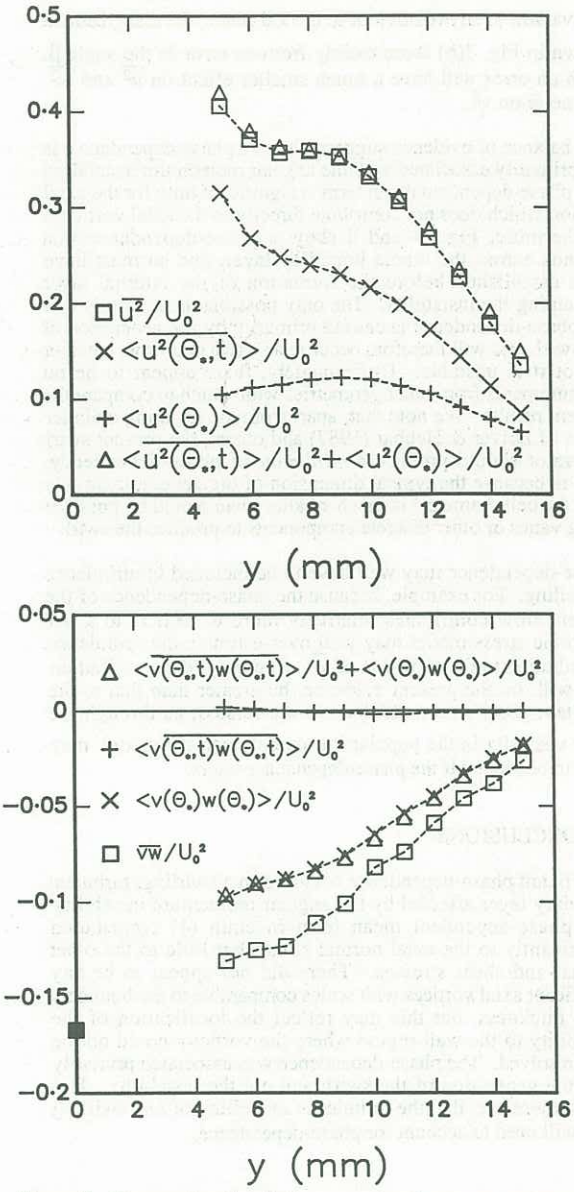


Figure 3. Conventional and phase-averaged stresses expressed as percentages. (a) $\overline{u^2}$, (b) $\overline{vw}$.

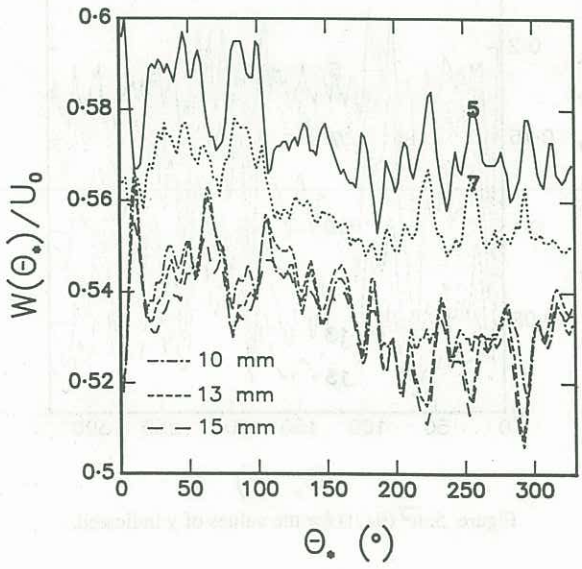


Figure 4. $W(\theta_*)$ for values of y indicated.

errors. The disagreement in the shear stresses would almost disappear if they were combined to give the resultant shear stress in the plane of the wall, $(\overline{uv}^2 + \overline{vw}^2)^{1/2}$. Since this stress is invariant to any rotation of in the x,θ-plane, the disagreement shown in Fig. 3(b) arose mainly from an error in the angle β. Such an error will have a much smaller effect on $\overline{u^2}$ and $\overline{w^2}$ and none on $\overline{v^2}$.

The balance of evidence suggests that the phase-dependenc e is *not* primarily associated with the angular momentum instability. The phase-dependent mean term is significant only for the axial motion which does not contribute directly to the axial vorticity. Furthermore, Fig.s 4 and 5 show a phase-dependence that extends across the whole boundary layer, and so must have been established before the formation of the internal layer containing the instability. The only possible deduction is that the phase-dependence is caused primarily by the generation of the swirl, and will therefore occur in any swirling flow, whether or not it is unstable. Unfortunately, there appear to be no measurements from other geometries with which to compare the present results. We note that, apart from the spinning cylinder flows of Driver & Hebbar (1987) and others, the present swirl generator should produce a *minimum* of phase-dependency. This is because the typical dimension of the generator (in this case the cell diameter) is much smaller than would be possible using vanes or other discrete components to produce the swirl.

Phase-dependence may well have to be included in turbulence modelling. For example, because the phase-dependence of the present flow contributes relatively more to $\overline{u^2}$ than to k, an algebraic stress model may well over-estimate the turbulence contribution to the diffusion of $\overline{u^2}$. Similarly, the contribution to k will, on the present evidence, be greater than that to the resultant shear stress. If the two are related, as through the eddy viscosity in the popular k-ε model, then the model may have to be altered if the phase-dependence alters.

## 4. CONCLUSIONS

Significant phase-dependence occurred in a swirling, turbulent boundary layer affected by the angular momentum instability. The phase-dependent mean term in equn (1) contributed significantly to the axial normal stress, but little to the other normal and shear stresses. There did not appear to be any significant axial vortices with scales comparable to the boundary layer thickness, but this may reflect the localization of the instability to the wall region where the vorticity could not be fully resolved. The phase-dependence was associated primarily with the generation of the swirl, and not the instability. It is likely, therefore, that the turbulence modelling of *any* swirling flow will need to account for phase-dependence.

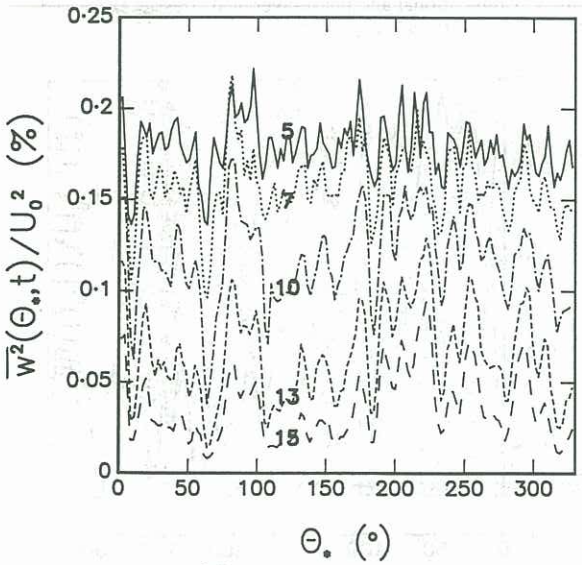


Figure 5. $\overline{w^2}$ ($\theta_*$, t) for the values of y indicated.


## ACKNOWLEDGEMENTS

This work was supported by the A.R.C. Most of the data acquisition software was written by Mr J.J. Smith.


## REFERENCES


S.D. ANDERSON and J.K. EATON (1989) *J. Fluid Mech.* **202**, 263.

V. BASKARAN and P. BRADSHAW (1988) *Expts in Fluids* **6**, 487.

P. BRADSHAW (1987) *Ann. Rev. Fluid Mech.* **19**, 53.

P.D. CLAUSEN (1988) Ph.D. Thesis, Univ. Newcastle.

P.D. CLAUSEN and D.H. WOOD (1987) in *Proc. 6th Symp. Turb. Shear Flows*, Toulouse.

P.D. CLAUSEN and D.H. WOOD (1989) *J. Fluids Engg* **111**, 226.

D. M. DRIVER and S.K. HEBBAR (1987) *A.I.A.A. J.* **25**, 35.

J.M. FLORYAN (1989) *A.I.A.A. J.* **27**, 112.

J.P. GOSTELOW (1977) *J. Eng. Power* **99**, 97.

A. HAGIWARA, S. BORTZ and R. WEBER (1986) doc. nr F259/a/3 Intl Flame Res. Foundation, IJmuiden, The Netherlands (1986).

P.H. HOFFMANN, K.C. MUCK and P. BRADSHAW (1985) *J. Fluid Mech.* **161**, 37.

J.D. HOOPER and D.H. WOOD (1984) *Nucl. Engg & Design* **83**, 31.

L. JACQUIN, O. LEUCHTER and P. GEFFROY(1987) in *Proc. 6th Symp. Turb. Shear Flows*, Toulouse.

B. LAKSHMINARAYANA (1981) *J. Eng. Power* **103**, 374.

R.D. MEHTA and P.H. HOFFMANN (1987) *Expts in Fluids* **4**, 358.

I.S. MILLER, D.A. SHAH and R.A. ANTONIA (1987) *J. Phys. E.* **20**, 311.

H.L. REED and W.S. SARIC (1989) *Ann. Rev. Fluid Mech.* **21**, 235.

A.J. SMITS and D.H. WOOD (1985) *Ann. Rev. Fluid Mech.* **17**, 321.

A.J. SMITS, S.T.B. YOUNG and P. BRADSHAW (1979) *J. Fluid Mech.* **94**, 209.

A.A. TOWNSEND (1976) The Structure of Turbulent Shear Flow, C.U.P. 2nd edn.

F.M. YOWAKIM and R.J. KIND (1988) *J. Fluids Engg* **110**, 257.


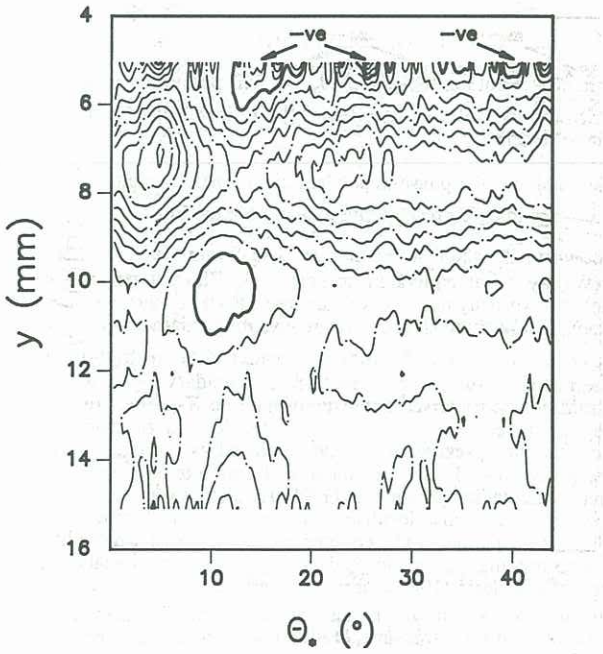


Figure 6. Contours of phase-dependent axial vorticity. Chain lines indicate positive vorticity; heavy, solid lines indicate zero vorticity and regions of negative vorticity are indicated. Contour increment is 40 $s^{-1}$.